Diagnosis of Variability and Trends in a Global Precipitation Dataset Using a Physically Motivated Statistical Model

M. R. P. Sapiano[1], D. B. Stephenson[1], H. J. Grubb[*], P. A. Arkin[+]

[1] Department of Meteorology, University of Reading

[*] School of Applied Statistics, University of Reading

[+] Earth Systems Science Interdisciplinary Center, University of Maryland

Submitted to the Journal of Climate

April 19, 2005

[1]M. R. P. Sapiano, Department of Meteorology, University of Reading, Earley Gate, PO Box 243, Reading RG6 6BB, U. K., E-mail: m.sapiano@reading.ac.uk

ABSTRACT

A physically motivated statistical model is used to diagnose variability and trends in Oct–Mar Global Precipitation Climatology Project (GPCP) pentad precipitation totals. Quasi-geostrophic theory suggests that extra-tropical precipitation amounts should depend multiplicatively on pressure gradient, saturation specific humidity and the meridional temperature gradient. This physical insight has been used to guide the development of a suitable statistical model for precipitation using a mixture of Generalized Linear Models: a logistic model for the binary occurrence of precipitation and a Gamma distribution model for the wet day precipitation amount.

The statistical model allows the investigation of the role of each factor in determining variations and long-term trends. Saturation specific humidity q_s has a generally negative effect on global precipitation occurrence and with tropical wet pentad precipitation amount, but has a positive relationship with pentad precipitation amount at mid and high latitudes. The North Atlantic Oscillation, a proxy for the meridional temperature gradient, is also found to have a statistically significant positive effect on precipitation over much of the Atlantic region. Residual time trends in wet pentad precipitation are extremely sensitive to the choice of wet pentad threshold because of increasing trends in low-amplitude precipitation pentads, too low a choice of threshold can lead to a spurious decreasing trend in wet-pentad precipitation amounts. However, for not too small thresholds, it is found that the meridional temperature gradient is

an important factor for explaining part of the long-term trend in Atlantic precipitation.

Key words: Precipitation, trends, statistics, generalized linear model, meridional temperature gradient, climate change

1. Introduction

Precipitation is an important weather element whose future changes will have a large impact on society (e.g. more droughts and floods). Recent flooding events in the United Kingdom such as those in October and November 2000 (DEFRA, 2001), November 2002 and January 2003 have brought this problem to the forefront of the public mind and have lead to substantial insurance losses (Hawes, 2003).

The Intergovernmental Panel on Climate Change concluded that global average surface temperature had increased by $0.6 \pm 0.2^{\circ}C$ over the 20^{th} century (IPCC, 2001) and that there is evidence that most of the warming observed over the last 50 years is attributable to human activities. However, there is less certainty associated with trends in precipitation. IPCC (2001) concluded that precipitation amounts have increased over much of the globe, with a decrease over subtropical areas, but that the detection of these trends is problematic because they are neither temporally nor spatially uniform (Folland *et al.*, 2001). Furthermore, the underlying cause of trends in regional precipitation remains unclear.

Global gauge/satellite precipitation datasets are available from 1979, but a careful sub-seasonal statistical analysis of such datasets has yet to be published in the mainstream literature. The main aim of this study is explore the dominant causes of variability in extra-tropical precipitation and investigate the effect of

these factors on global precipitation trends.

Precipitation is highly discontinuous and occurs only during wet events which have non-uniform duration, frequency and intensity. These events aggregate to form the daily and monthly rainfall totals routinely measured at individual stations and much of the work on trends in precipitation has concentrated on the analysis of seasonal mean precipitation since this has a more Gaussian (Normal) distribution that is amenable to simple analysis techniques. However, seasonal mean precipitation is far removed from the sub-daily time-scales of the underlying processes.

A common failing of statistical studies is to select the model based only on the available data. A major aim of this study has been to use physical insight to inform the choice of the statistical model as well as the explanatory variables. Therefore, we present a physically-motivated probability model for precipitation across the globe. The physical motivation is also used to identify the most important factors for explaining precipitation variations. The statistical model can then be used to study how these factors help account for the long-term time trends in precipitation.

This article is structured as follows. Section a uses quasi-geostrophic theory to identify the key factors affecting extra-tropical large-scale winter precipitation. The main factors are local sea-level pressure (SLP), saturation specific humidity q_s and the meridional temperature gradient. The physical motiva-

tion is then used to develop a suitable statistical model in Section b. The chosen method models the probability of the occurrence of precipitation with a Bernoulli distribution and then separately models the wet pentad precipitation amount with a Gamma distribution. The Bernoulli and Gamma distributions are allowed to depend on explanatory factors using an extended regression approach known as Generalized Linear Modelling (GLM) (Nelder and Wedderburn, 1972). The model fitting is described in Section c. The pentad data is described in Section 3. Section 4 then applies the mixture GLM to precipitation at each gridpoint of Oct-Mar winter pentad Global Precipitation Climatology Precipitation (GPCP). Sea-level pressure and saturation specific humidity are used as explanatory factors as is the North Atlantic Oscillation which is used as a proxy for the meridional temperature gradient.

2. A physically motivated statistical model for diagnosis of precipitation

a. Physical considerations

The time-averaged vertically-averaged water budget can be written as

$$\int_{p_c}^{p_t} \nabla.(\overline{q}\overline{\mathbf{v}})\mathrm{d}p + [\overline{\omega q_s}]_{p_c}^{p_t} = \overline{e} - \overline{c}$$

where q is specific humidity, $\mathbf{v}$ is the horizontal component of vector velocity, p is pressure, ω is vertical velocity in pressure coordinates, e and c represent atmospheric evaporation and condensation and p_c and p_t represent pressure at

the condensation level and the top of the troposphere respectively (Peixoto and Oort, 1992).

The horizontal divergence term is generally small in comparison to the other terms. Since evaporation is generally small above the condensation level, the right hand side is approximately the rate of precipitation. Assuming that the air is fully saturated above the condensation level, the precipitation rate can be approximated by $\overline{q_s \omega}$, where q_s is saturation specific humidity. This can be expressed in S.I. units of ms^{-1} by multiplying this by the density of air, ρ_a, and dividing by the density of water, ρ_w and using vertical velocity in ms^{-1} as

$$\frac{\rho_a \overline{q_s w}}{\rho_w} \tag{1}$$

This expression can be used to obtain a rough estimate of the precipitation rate during the passage of an extra tropical cyclone. Typical extra-tropical cyclone values of $\rho_w \sim 10^3 kg\,m^{-3}$, $\rho_a \sim 1 kg\,m^{-3}$, $\overline{q}_s \sim 10^{-2} kg/kg$, $w \sim 10^{-2} m\,s^{-1}$ give a precipitation rate of $\sim 10^{-7}\ ms^{-1}$, equivalent to a value of 10 $mm\,day^{-1}$ that is typically observed.

Saturation specific humidity q_s is given by $q_s = \varepsilon e_s / p$ where $\varepsilon = 0.6213$ is the ratio of the molar masses of dry air and water vapour, and p is pressure and e_s is saturation vapour pressure. The saturation vapour pressure e_s is exponentially related to temperature by the Clausius-Clapeyron equation (Rogers and Yau, 1989).

Quasi-geostrophic theory can be used in the extra-tropics to estimate the vertical velocity, ω, in terms of the geostrophic wind. This diagnostic equation is known as the *omega equation* (Hoskins *et al.*, 1978, Durran and Snellman, 1987). The terms representing the horizontal advection of vorticity and thermal advection in the omega equation are often of similar magnitude, and opposite sign and often cancel each other out (Hoskins *et al.*, 1978, Trenberth, 1978). Hoskins *et al.* (1978) introduced the Q-vector approach, where the Q-vector is equal to the rate of change of the horizontal potential temperature gradient, which would develop in a fluid parcel moving with the geostrophic wind if the vertical velocity was exactly zero (Durran and Snellman, 1987).

The omega equation can be written in Q-vector form as:

$$\left[\sigma\nabla_h^2 + f^2\frac{\partial^2}{\partial p^2}\right]\omega = -2\nabla.\underline{Q} \tag{2}$$

where f is the Coriolis parameter, σ is the static stability which is a function of the basic state temperature in the mid-troposphere and $\underline{Q}$ is the 2-dimensional Q-vector given by

$$\underline{Q} = \left[\frac{\partial \mathbf{v}_g}{\partial x}.\nabla\left(\frac{\partial\Phi}{\partial p}\right), \frac{\partial \mathbf{v}_g}{\partial y}.\nabla\left(\frac{\partial\Phi}{\partial p}\right)\right] \tag{3}$$

Convergent $\underline{Q}$ is associated with ascent, whereas divergent $\underline{Q}$ is associated with subsidence (Hoskins and Pedder, 1980). Sanders and Hoskins (1990)

showed that (3) can be rewritten more simply as

$$\underline{Q} = -\frac{R}{P}\frac{\partial T}{\partial y}\nabla v_g \tag{4}$$

where v_g is the meridional geostrophic wind component and $\frac{\partial T}{\partial y}$ is the meridional temperature gradient in the mid-troposphere (e.g. at $500hPa$). Rewriting in terms of time mean and transient components gives

$$\underline{Q} = -\frac{R}{P}\frac{\partial \overline{T}}{\partial y}\nabla \overline{v} - \frac{R}{P}\frac{\partial \overline{T}}{\partial y}\nabla v' - \frac{R}{P}\frac{\partial T'}{\partial y}\nabla \overline{v} - \frac{R}{P}\frac{\partial T'}{\partial y}\nabla v' \tag{5}$$

It is reasonable in mid-latitudes to assume that $\overline{v} \ll v'$ and $\frac{\partial T'}{\partial y} \ll \frac{\partial \overline{T}}{\partial y}$ and so

$$\underline{Q} \approx -\frac{R}{P}\frac{\partial \overline{T}}{\partial y}\nabla v' \tag{6}$$

Therefore

$$\omega \approx \left[\sigma\nabla^2 + f^2\frac{\partial^2}{\partial p^2}\right]^{-1}\left[\frac{2R}{f\rho p}\frac{\partial \overline{T}}{\partial y}\nabla^2\frac{\partial p'}{\partial x}\right] \tag{7}$$

Equation (7) shows that ω is a function of the transient pressure anomaly p', the time-mean meridional temperature gradient $\frac{\partial \overline{T}}{\partial y}$ and the static stability σ. Hence, a stronger meridional temperature gradient will increase vertical velocities for a given pressure anomaly p'. Static stability has an inverse effect on vertical motion – reduction in static stability will enhance vertical velocities. Note that

static stability is also a possible factor, but previous studies suggest that this is unlikely to change substantially beyond natural variability (Pavan *et al.*, 1999). Equations (1) and (7) suggest that precipitation is the product of saturation specific humidity, pressure anomaly and meridional temperature gradient.

The dry quasi-geostrophic equations neglect certain terms contained in the primitive equations, such as enhanced vertical motion due to diabatic processes (the release of latent heat) and frictional effects. Räisänen (1995) compared the quasi-geostrophic omega equation with a hydrostatic generalized omega equation and found a correlation of 0.7 between the ω estimated using the quasi-geostrophic and generalized omega equations in mid-latitudes. Räisänen (1995) concluded that, whilst the dominant causes of vertical motion in the mid-latitudes are vorticity and thermal advection, the effect from diabatic heating is far from negligible. Therefore, the quasi-geostrophic omega equation provides a good first order approximation for estimating synoptic scale vertical velocities, but a more detailed treatment that includes diabatic effects may be required for smaller scale effects such as those that dominate in the warm season. Note also that the quasi-geostrophic approximation only applies in the extra-tropics, and that factors affecting tropical precipitation might be different to those in the extra-tropical cold season.

b. A statistical model for precipitation

Coe and Stern (1982) suggested a two-component mixture model for modelling the occurrence of precipitation and the precipitation amount on a wet day. Binary precipitation occurrence, $W = 0$ or 1, was modelled as a Bernoulli distribution $P(W = w) = \pi^w(1-\pi)^{(1-w)}$. Wet days were defined as days on which the precipitation amount exceeded a small threshold y_0. The precipitation amount on a wet day was modelled using a Gamma distribution with mean μ and constant shape parameter ν. The parameters π and μ can be made to depend on explanatory variables $x_1, x_2, \ldots, x_p$. This model provides a method for exploring the effect of the identified factors on precipitation, and is multiplicative due to the log link. This type of model has been used in several previous studies (Stern and Coe, 1984, Buishand and Tank, 1996, Brandsma and Buishand, 1997, Buishand and Brandsma, 1999, Chandler and Wheater, 2002) but not for investigating trends and variations in global precipitation datasets.

The binary response variable W is Bernoulli distributed with a *log-odds* (i.e. the log of the probability of an event, divided by the probability that it does not occur) that depends on a linear combination of explanatory variables. The occurrence of precipitation W is modelled using a *logistic* regression given by

$$\begin{aligned} W|\eta &\sim \mathrm{Be}(\pi) \\ \log\left(\tfrac{\pi}{1-\pi}\right) = \eta &= \lambda_0 + \lambda_1 x_1 + \ldots + \lambda_j x_j + \ldots + \lambda_p x_p \end{aligned} \tag{8}$$

where $W = 1$ on a wet day and $W = 0$ otherwise. The non-linear link function $\log\left(\frac{\pi}{1-\pi}\right)$ is linearly related to the p explanatory variables with $p+1$ intercept and slope parameters, λ_j ($j = 0, \ldots, p$).

One of the main problems of GLMs is that the model parameters are not generally on the same scale as the response due to the non-linear link function (e.g. $g(\pi) = \log(\pi/1-\pi)$ in Eqn. 8). The parameters can be presented informatively by showing the change in the response due to a unit increase in the explanatory variable. For example, the odds $\pi/1-\pi$ is given by $\exp(\lambda_0 + \lambda_1 x_1 + \ldots + \lambda_p x_p)$ and so a unit change in x_1 will cause the odds to change by a factor of e^{λ_1}. Hence, $(e^{\lambda_1} - 1) \times 100$ gives the percentage change in the odds of precipitation for a unit change in x_1.

The wet day precipitation amount Y_w is modelled using a Gamma distribution as follows:

$$\begin{aligned} Y_w|\eta &\sim \text{Gamma}(\mu, \nu) \\ \log(\mu) = \eta &= \kappa_0 + \kappa_1 x_1 + \ldots + \kappa_j x_j + \ldots + \kappa_p x_p \\ \nu &= \text{constant} \end{aligned} \tag{9}$$

where Gamma$(.)$ represents the Gamma distribution. The log of the mean wet day precipitation, $\log(\mu)$, is linearly related to the p explanatory variables by $p+1$ parameters, κ_j ($j = 0, \ldots, p$). See Nelder and Wedderburn (1972) for further discussion of this GLM. By using a logarithmic link, the factors affecting

the wet day mean precipitation amount become multiplicative as suggested by the physical arguments presented earlier. The assumption of constant shape ν implies a constant coefficient of variation (the ratio of the mean and the standard deviation) for fixed values of $x_1, \ldots, x_p$.

Because of the logarithmic link function, the parameters are not on the same scale as the response. The parameters can be expressed in terms of the unit change in response due to a unit change in any of the explanatory variables. For example, the percentage unit change in μ due to a unit change in x_1 is given by $(e^{\kappa_1} - 1) \times 100$.

c. Estimation of the model parameters

The mixture model has been fitted to global gridded estimates of October–March precipitation. At each gridpoint, the parameters of the mixture model were estimated independently of the other gridpoints. Since an extended winter is to be used, sine and cosine explanatory variables in calendar day were also included in the models to account for the fixed annual cycle. All explanatory variables have been fitted as anomalies to their long-term mean so that the intercept represents the mean wet pentad odds for the occurrence model and the mean wet pentad precipitation amount in the wet pentad precipitation model, both of which will be taken for the year 2003. A long-term residual time trend is included by also adding the year as an explanatory variable in the model. All parameters are assumed to be stationary in time, although non-stationarity could

be examined by the inclusion of interaction terms. Such interaction terms have not been included here, since this would lead to a much more complex model.

An advantage of a parametric model-based statistical approach is that it allows the statistical significance of the parameters in the model to be rigorously tested. Although for brevity the statistical significance of the parameters will not be shown here, only relationships which are at least statistically significant at the 5% level will be discussed.

The study of precipitation using the mixture GLM requires the selection of a wet pentad threshold. Since precipitation magnitude varies considerably across the globe, a spatially variable threshold is desirable. The threshold has been defined here using the 25^{th} percentile of the wet pentad distribution at each gridpoint. This is later compared with a globally uniform threshold of 0.1 *mm/day*. The higher 25^{th} percentile threshold is required to eliminate the effect of spurious trends in light precipitation.

3. Data

a. The response variable: precipitation

The Global Precipitation Climatology Project (GPCP) pentad precipitation dataset is a merged satellite/gauge estimate of global precipitation on a grid with 2.5° by 2.5° spatial resolution (Xie *et al.*, 2003). The dataset used here covers the period 1979–2001. Since the available satellite data covers a relatively short

time period, an extended Oct–Mar winter analysis has been used in order to increase the sample size to 792 pentads. Similar results are obtained using a shorter Dec–Feb winter season (not shown), but the resulting fields are noisier. The GPCP global precipitation dataset (which will be referred to as simply GPCP) is used as the primary dataset for global analysis, since it is the longest global record with pentad temporal resolution.

Figure 1

Figure 1 shows the mean pentad precipitation for Oct–Mar winters from 1979 to 2001. The maximum precipitation occurs around the tropical convergence zones. Noteworthy features include the inter-tropical convergence zone (ITCZ) just north of the equator, the precipitation maxima over northern parts of South America and Central Africa, the arid desert regions of North Africa and Southern Asia and the dry subtropical regions of ascent over the oceans in the Southern Hemisphere. In mid-latitudes, precipitation is dominated by extratropical cyclones and is maximum in storm tracks over the Atlantic and Pacific oceans. Precipitation in high latitudes is generally low.

b. The explanatory variables: pressure, humidity and temperature gradient

Sea-level pressure, saturated specific humidity and meridional temperature gradient were identified as explanatory variables for the statistical modelling in Section a.

I. SEA-LEVEL PRESSURE

Local sea-level pressure series at each gridpoint have been obtained from the European Center for Medium-range Weather Forecasts (ECMWF) ERA-40 reanalysis (Simmons and Gibson, 2000). The fine resolution ERA-40 analysis data was transferred to the coarser GPCP grid using linear interpolation.

II. SATURATION SPECIFIC HUMIDITY

Figure 2

Saturation specific humidity can be calculated from saturation vapour pressure. A simple method of calculating saturation vapour pressure from temperature and SLP was presented by Murray (1967). This method was used here to combine SLP and 2m temperature data obtained from the ERA-40 reanalysis to yield global gridded values of derived q_s. Figure 2 shows the linear time trend in Oct–Mar winter mean q_s over the period 1979 to 2001. The trends in q_s closely follow trends in temperature. Folland *et al.* (2001) showed the mean DJF temperature trends over the globe from 1976 to 2001. The main features of Fig. 2 are similar to those shown by Folland *et al.* (2001), with positive trends over Europe and much of the Atlantic, and a mix of positive and negative trends over the Pacific. However the large positive trend over Central Asia reported by Folland *et al.* (2001) is not evident in saturated humidity, and the trend over the north-west of North America has the opposite sign to that in Folland *et al.*

(2001). The large negative trend over much of the Pacific Ocean is smaller and does not extend as far spatially in the analysis of Folland *et al.* (2001). Investigation of the ERA-40 DJF $2m$ temperature trend (not shown) reveals that the differences in sign are mainly caused by the influence of October, November and March in the extended boreal winter analysis, but that the lower magnitudes in the trends over Russia and the north-west of North America are possibly due to the different time period used by Folland *et al.* (2001).

III. Meridional temperature gradient

Away from the equator, the meridional temperature gradient (MTG) in Eqn. (4) is related to the vertical shear in the zonal wind by the thermal wind relation

$$\frac{\partial \overline{u}_g}{\partial p} = \frac{R}{fp}\frac{\partial \overline{T}}{\partial y} \tag{10}$$

where u_g is the geostrophic zonal wind and p is the vertical pressure coordinate. The strongest zonal wind shear occurs in regions with the strongest meridional temperature gradients. By geostrophy, the zonal wind is in turn related to the meridional gradient in geopotential height as follows

$$\overline{u}_g = -\frac{g}{f}\frac{\partial \overline{Z}}{\partial y} \tag{11}$$

where Z is geopotential height. Hence, the meridional gradient in geopotential

height (or sea-level pressure) as estimated by the NAO index provides a measure of the strength of the zonal flow and hence the meridional temperature gradient (see Wanner *et al*., 2001, and Stephenson *et al*., 2003, for reviews of the NAO). When NAO is strongly positive, the zonal flow in the N. Atlantic is stronger than normal and there is a stronger meridional temperature gradient in the upper troposphere. Hence, from the omega equation, one should expect more precipitation for a given vertical velocity during periods when NAO is strongly positive. This dynamical effect of the NAO on precipitation is in addition to NAO's effect on northward steering of North Atlantic storms.

The link between the NAO and European precipitation is supported by several authors who have linked the north-south shift of the storm-tracks to precipitation (Hurrell, 1995, Türkeş and Erlat, 2003, Uvo, 2003, Trigo *et al.*, 2004). However, Eqn. (7) shows that the NAO is also related to increased *precipitation intensity* due to a strengthened MTG.

Jones *et al.*, (2003) reviewed methods for monitoring the NAO. The simplest approach is to calculate the difference in mean SLP at points over Iceland and the Azores. A more robust approach is to take the first Principal Component (PC) time series of regional (or Northern Hemispheric) SLP. Barnston and Livezey (1987) calculated an NAO index based on a rotated principal components analysis of Northern Hemispheric mean 700 *hPa* geopotential height. This series will be used here as a proxy for the meridional temperature gradient. The daily Climate Prediction Center (CPC) series has been averaged here to make

pentad means.

4. Results

Figure 3 Figure 4

Figure 3 shows the estimated mean wet pentad precipitation amount $e^{\hat{\kappa}_0}$. As might be expected, the mean wet pentad precipitation has a similar global pattern to the mean precipitation shown in Fig. 1. Fig. 3 highlights areas where the precipitation is particularly intense when it does occur, such as over the rainforests and in the tropics. Figure 4 shows the estimated shape parameter ν at each gridpoint. In general, areas with a high mean precipitation also have a large shape parameter. A Gamma distribution with a shape parameter greater than unity resembles the normal distribution with a slight positive skew. This behaviour is seen over much of the globe in Fig. 4. A Gamma distribution with a shape parameter less than or equal to unity is monotonically decreasing (inverted J-shape) and occurs in Fig. 4 in extremely dry areas such as the deserts, the subtropics and the Southern Hemisphere oceanic subsidence regions.

a. Dependence on SLP

Figure 5

Figure 5a shows the SLP parameter estimate $(e^{\hat{\lambda}_1} - 1) \times 100\%$ across the globe. Since the variability of SLP is meridionally inhomogeneous, SLP has

been standardized by its own standard deviation in the model. This allows for comparison of different areas of the globe, although the units become percentage change *per standard deviation*. note that this does not have any effect on the sign or the statistical significance of the parameter, but can alter the magnitude. There is a strong negative relationship between the odds of precipitation occuring and SLP over nearly all of the globe. Notable exceptions appear over the tropics where convection dominates. The negative relationship can reach up to a 50% reduction in the odds of precipitation for a one standard deviation change in SLP. Fig. 5b shows the SLP parameter estimates $(e^{\hat{\kappa}_1} - 1) \times 100\%$ for wet pentad precipitation amount. As with the model for the precipitation occurrence, the relationship between the wet pentad precipitation and SLP is negative over much of the globe. There is very little evidence of a relationship between SLP and precipitation amount over the tropics. However, there is a small intriguing positive relationship on the poleward side of the storm tracks.

b. Dependence on humidity

Figure 6

Figure 6a shows the q_s parameter estimates $(e^{\hat{\lambda}_2} - 1) \times 100\%$ for precipitation occurrence. The relationship is negative and statistically significant over much of the globe – higher humidity leads to a lower chance of a wet pentad. This could be due to the increased capacity of the air for holding moisture: warmer air has a higher saturation specific humidity, so that larger vertical motions are

required to reach saturation. Hence condensation (and therefore precipitation) is suppressed by high q_s due to the increased water holding capacity of the air. The relationship is positive at high latitudes – higher humidity increases the chance of a wet pentad. Figure 6b shows the q_s parameter estimates $(e^{\hat{\kappa}_2} - 1) \times 100\%$ for precipitation occurrence. There is a positive relationship over parts of Europe and the North Atlantic region but the most striking relationship is over the tropics, particularly the Pacific Ocean. This relationship implies that increasing q_s might be responsible for increased precipitation in mid-latitudes if there was more available water.

c. Dependence on meridional temperature gradient

Figure 7

Figure 7a shows the NAO parameter estimates $(e^{\hat{\lambda}_3} - 1) \times 100\%$ for the occurrence of precipitation. Over much of the globe, there is not a strong statistically significant response. However over the North Atlantic region, there is a positive response to the NAO which shows that NAO positive behaviour leads to increased chance precipitation. There is some evidence of a tripole pattern with a non-local NAO response over the mid-Atlantic. Trigo *et al.* (2004) showed that there is a negative relationship between precipitation over the Iberian peninsula and the NAO which is consistent with the weak centre of the dipole. The positive response over the mid-Atlantic is perhaps due to the enhanced easterlies associated with the NAO and the strengthening of the African Easterly jet.

Figure 7b shows the NAO parameter estimates $(e^{\hat{\kappa}_3} - 1) \times 100\%$ for the wet pentad precipitation amount. There is a large positive relationship over much of the Atlantic. The pattern observed here is similar to that in Fig. 7a with a tripole pattern over the East Atlantic, except that the relationship for wet pentad precipitation is weaker over the North Atlantic for the wet pentad precipitation amount. Therefore, in addition to local SLP, NAO enhances both the occurrence and intensity of precipitation over much of the Atlantic region.

d. Residual time trends

Figure 8

The estimation of long-term trend in the data is difficult due to the short period available. It is also important to note that time trends can be due to interdecadal climate variability rather than secular climate change. Figures 8a and 8b show the time trend estimates in the odds of precipitation and the wet pentad precipitation amount from the models with only the annual cycle and the time trend but with the wet pentad threshold set to a constant 0.1 *mm/day*. Fig. 8c and Fig. 8d show the same fields, but for a threshold defined by the 25^{th} percentile. The fixed threshold of 0.1 *mm/day* represents the lowest physically plausible wet pentad threshold, and the 25^{th} percentile represents a spatially variable higher threshold. Comparison of Fig. 8a and Fig. 8c shows that the low fixed threshold gives positive trends over much of the globe, in contrast to the more negative trends for the higher variable threshold. The time trends in

Fig. 8b are generally negative over the UK. Contrary to this, the trends obtained using a variable threshold in Fig. 8d are more positive. Decreases in dry pentad occurrence are compensated by increases of low intensity wet pentad events (drizzle). The increase in low intensity wet pentad events gives the impression that the mean of the wet pentad amounts is decreasing, whereas in fact larger amplitude wet pentad amounts are increasing in intensity.

Figures 8e and 8f show time trend estimates in the odds of precipitation and the wet pentad precipitation amount from the models with all the explanatory variables included and with a wet pentad threshold defined by the 25^{th} percentile. Comparison of Figs. 8e and 8f with 8c and 8d allows one to assess how much of the long-term time trend can be explained by the explanatory factors. The time trend is shown as the percentage change in the odds of a wet day $(e^{\hat{\kappa}_3} - 1)100\%$. Therefore, a 5% increase in odds of 4 to 1 changes the odds to 4.2 to 1 (or 21 to 5), although the areas with time trends this large are unlikely to represent long-term trend. Fig. 8c shows that there has been a decreasing trend in precipitation occurrence over the North Atlantic and over large parts of the Pacific ocean. These patterns change slightly with the addition of the other explanatory variables (shown in Fig. 8e). The trend in precipitation occurrence is more negative over the North Atlantic and Europe and decreased the trends slightly over the North Pacific and the USA. Fig. 8d shows the time trends in the wet pentad precipitation. There are generally small trends in mid-latitudes, with slightly larger trends over tropical areas. There is a weak negative trend over

mid-latitude continental areas, with positive trends over mid-latitude oceanic areas and the tropics (particularly in the El Niño region). Folland *et al.* (2001) reported a general global increase since 1900, and Fig. 8d agrees with this as the time trends are generally positive. The time trends in the wet pentad amount change slightly with the inclusion of SLP, q_s and the NAO (shown in Fig. 8f). Most interestingly, the trend over the North Atlantic region becomes more negative for the full model. This shows that SLP, q_s and the NAO explain some but not all of the long-term trend in precipitation amounts.

5. Conclusions

It has been argued here that the vertical velocity of ascending air and humidity are important multiplicative factors for large-scale, winter, extra-tropical precipitation. The quasi-geostrophic ω-equation was used to show that mid-tropospheric meridional temperature gradient is also an important (yet often neglected) factor for large-scale vertical motion in the extra-tropics. It was also shown that these factors have a multiplicative effect on precipitation amount, and so statistical analyses of precipitation should respect this multiplicative property.

Local SLP, saturation specific humidity, and MTG are all physically motivated and statistically significant (at 10% level) factors for accounting for variations in Oct-Mar pentad precipitation amounts. SLP was found to have a strong negative effect on both precipitation occurrence and the wet pentad

amount over much of the globe, except in the tropics, and on the poleward side of the stormtracks where the relationship was slightly positive. There was a generally negative effect of q_s on precipitation occurrence with exceptions over the tropical Pacific region, the deserts of North Africa and Southern Asia and around the Northern Hemisphere storm tracks, where there was a positive relationship. There was a positive effect of q_s on the wet pentad precipitation amount over mid- and high-latitudes and the tropical Pacific, and a negative relationship over the rest of the tropics. The NAO, a proxy for the MTG, was found to be a statistically significant positive factor in addition to local SLP over the Atlantic Ocean for explaining both wet pentad occurrence and wet pentad amount. These results regarding the relationships between precipitation and some of the important explanatory factors might also be of further use in evaluation of model performance for climate modelling studies.

A negative long-term time trend was found in wet day occurrence in GPCP precipitation over 1979–2001 over the North Atlantic and parts of the Pacific Ocean with less coherent patchy trends over much of the globe. There was a generally increasing trend in wet day amount over the North Atlantic and much of the Pacific Ocean with decreases over Europe and North America. Saturation specific humidity and MTG are able to explain some but not all of the long-term linear time trend in precipitation. SLP trends fail to explain the increasing trends in precipitation amount over the North Atlantic region. The long-term time trends in precipitation are rather sensitive to the choice of threshold espe-

cially when the threshold is small. Time trends in the precipitation amount can be misleading when too low a threshold is applied. Increasing trends in low-intensity precipitation can lead to a spurious decreasing trend in wet-pentad precipitation totals. The problem in the low threshold model is most likely an artifact of the detection method, since many satellite techniques have difficulty in accurately representing low precipitation amounts. This problem is likely to be of reduced impact in more recent merged satellite records, such as those after 1987 after the introduction of SSM/I.

Whilst the explanatory variables have been shown to account for some of the long-term time trend, they do not currently account for all of it. This suggests either that other factors are important (such as static stability), or that the long-term time trends in GPCP are inconsistent with other datasets. The estimation of long-term time trends is complicated by the relatively short period covered by GPCP, and the trends are not always consistent with longer, more localized, precipitation studies (such as over the UK, e.g. Jones and Conway, 1997). Careful comparison of GPCP with longer regional or station based datasets might be required to verify some of the trends over the short period. Another drawback of this approach is the sensitivity of time trends to the arbitrary choice of threshold. This might be addressed by the development of a method for estimating the wet pentad threshold based on goodness of fit of the Bernoulli and Gamma distributions to the data.

Acknowledgements

We wish to acknowledge Prof A. J. Thorpe and Prof B. J. Hoskins who both provided useful and insightful comments on some of this work. MRPS was supported by the Natural Environmental Research Council and a bursary from the Department of Meteorology, University of Reading.

REFERENCES

Barnston, A. G. and R. E. Livezey, 1987: Classification, Seasonality and Persistence of Low-Frequency Atmospheric Circulation Patterns. *Monthly Weather Review*, **115**(6), 1083–1126.

Brandsma, T. and T. A. Buishand, 1997: Statistical Linkage of Daily Precipitation in Switzerland to Atmospheric Circulation and Temperature. *Journal of Hydrometeorology*, **198**(1-4), 98–123.

Buishand, T. A. and T. Brandsma, 1999: Dependence of Precipitation on temperature at Florence and Livorno (Italy). *Climate Research*, **12**, 53–63.

Buishand, T. A. and A. M. G. K. Tank, 1996: Regression Model for Generating Time Series of Daily Precipitation Amounts for Climate Change Impact Studies. *Stochastic Hydrology and Hydraulics*, **10**(2), 87–106.

Chandler, R. E. and H. S. Wheater, 2002: Analysis of Rainfall Variability using Generalized Linear Models: A Case Study from the West of Ireland. *Water Resources Research*, **38**(10), art. no. 1192.

Coe, R. and R. D. Stern, 1982: Fitting Models to Daily Rainfall Data. *Journal of Applied Meteorology*, **21**, 1024–1031.

DEFRA, 2001: To what degree can the October/November 2000 flood events be attributed to climate change? Tech. Rep. FD2304 Final Report, DEFRA, Department for Environment, Food & Rural Affairs, Nobel House, 17 Smith

Square, London, SW1P 3JR. 35 pp.

Durran, D. R. and L. W. Snellman, 1987: The Diagnosis of Synoptic-Scale Vertical Motion in an Operational Environment. *Weather and Forecasting*, **2**, 17–31.

Folland, C., T. Karl, J. Christy, R. Clarke, G. Gruza, J. Jouzel, M. Mann, J. Oerlemans, M. Salinger, and S. Wang, 2001: *Climate Change 2001: The Scientific Basis. Contribution of Working Group I to the Third Assessment Report of the Intergovernmental Panel on Climate Change*, chapter Observed Climate Variability and Change, pages 99–181. Cambridge University Press. (ed. J. T. Houghton, Y. Ding, D. J. Griggs, M. Noguer, P. J. van der Linden, X. Dai, K. Maskell and C. A. Johnson).

Hawes, G., 2003: Property Insurance in the UK - What Does the Future Hold? *FloodRiskNet Newsletter*, http://www.floodrisknet.org.uk/, Issue 2, Winter 2003, pages 9–10.

Hoskins, B. J. and M. A. Pedder, 1980: The Diagnosis of Middle Latitude Synoptic Development. *Quarterly Journal of the Royal Meteorological Society*, **106**, 707–719.

Hoskins, B. J., I. Draghici, and H. C. Davies, 1978: A new look at the ω-equation. *Quarterly Journal of the Royal Meteorological Society*, **104**, 31–38.

Hurrell, J. W., 1995: Decadal trends in the North Atlantic Oscillation: Regional

temperatures. *Science*, **269**(5224), 676–679.

Jones, P. D. and D. Conway, 1997: Precipitation in the British Isles: an Analysis of Area-Average Data Updated to 1995. *International Journal of Climatology*, **17**, 427–438.

Jones, P. D., T. J. Osborn, and K. R. Briffa, 2003: Pressure-Based Measures of the North Atlantic Oscillation (NAO): A Comparison and an Assessment of Changes in the Strength of the NAO and its Influence on Surface Climate Parameters. In J. W. Hurrell, Y. Kushnir, G. Ottersen, and M. Visbeck, editors, *The North Atlantic Oscillation: Climatic Significance and Environmental Impact*, pages 51–62. American Geophysical Union, Washington, DC.

Murray, F. W., 1967: On the Computation of Saturation Vapor Pressure. *Journal of Applied Meteorology*, **6**(1), 203–204.

Nelder, J. A. and R. W. M. Wedderburn, 1972: Generalized Linear Models. *Journal of the Royal Statistical Society. Series A (General)*, **135**(3), 370–384.

Pavan, V., N. Hall, P. Valdes, and M. Blackburn, 1999: The Importance of Moisture Distribution for the Growth and Energetics of Mid-latitude Systems. *Annales Geophysicae - Atmospheres and Space Sciences*, **17**(2), 242–256.

Peixoto, J. P. and A. H. Oort, 1992: *Physics of Climate*. American Institute of Physics, New York. 520 pp.

Räisänen, J., 1995: Factors Affecting Synoptic-scale Vertical Motions: A Sta-

tistical Study using a Generalised Omega Equation. *Monthly Weather Review*, **123**, 2447–2460.

Rogers, R. R. and M. K. Yau, 1989: *A Short Course in Cloud Physics*. Pergamon, Oxford, 3rd edition. 290 pp.

Sanders, F. and B. J. Hoskins, 1990: An Easy Method for Estimation of Q-vectors from Weather Maps. *Weather and Forecasting*, **5**, 346–353.

Simmons, A. J. and J. K. Gibson, 2000: The ERA-40 Project Plan. *ERA-40 Project Report Series, 1*. ECMWF, Reading, UK.

Stephenson, D. B., H. Wanner, S. Brönnimann and J. Luterbacher, 2003: The History of Scientific Research on the North Atlantic Oscillation. In J. W. Hurrell, Y. Kushnir, G. Ottersen, and M. Visbeck, editors, *The North Atlantic Oscillation: Climatic Significance and Environmental Impact*. American Geophysical Union, Washington, DC, pages 37–50.

Stern, R. D. and R. Coe, 1984: A Model Fitting Analysis of Daily Rainfall Data. *Journal of the Royal Statistical Society. Series A (General)*, **147**(1), 1–34.

Trenberth, K. E., 1978: On the Interpretation of the Diagnostic Quasi-Geostrophic Omega Equation. *Monthly Weather review*, **106**, 131–137.

Trigo, R. M., D. Pozo-Vázquez, T. J. Osborn, Y. Castro-Díez, S. Gámiz-Fortis, and M. J. Esteban-Parra, 2004: North Atlantic Oscillation Influence on Precipitation, River Flow and Water Resources in the Iberian Peninsula. *International*

Journal of Climatology, **24**, 925–944.

Türkeş, M. and E. Erlat, 2003: Precipitation Changes and Variability in Turkey Linked to the North Atlantic Oscillation During the Period 1930-2000. *International Journal of Climatology*, **23**, 1771–1796.

Uvo, C. B., 2003: Analysis and Regionalization of Northern European Winter Precipitation Based on its Relationship with the North Atlantic Oscillation. *International Journal of Climatology*, **23**, 1185–1194.

Wanner, H., S. Bronnimann, C. Casty, D. Gyalistras, J. Luterbacher, C. Schmutz, D. B. Stephenson and E. Xoplaki, 2001: North Atlantic Oscillation - Concepts and Studies. *Surveys in Geophysics*, **22**(4), 321–382.

Xie, P., J. E. Janowiak, P. A. Arkin, R. Adler, A. Gruber, R. Ferraro, G. J. Huffman and S. Curtis, 2003: GPCP Pentad precipitation analyses: An experimental dataset based on gauge observations and satellite estimates. *Journal of Climate*, **16**(13), 2197–2214.

FIGURE CAPTIONS

Figure 1: Long-term mean of October–March winter GPCP pentad precipitation for the period 1979–2001. Units: *mm/day*.

Figure 2: Long-term linear time trend in October–March saturated specific humidity over the period 1979–2001. Units: *g/kg* per year. 1-2-1 smoothing applied for lisability. Solid lines indicate positive contours starting at 0.01 *g/kg* with dashed lines and shading to indicate negative contours starting at -0.01 *g/kg*. Contour interval is 0.02 *g/kg* and the zero line has been omitted.

Figure 3: Long-term mean of October–March winter GPCP wet pentad precipitation amount $e^{\hat{\kappa}_0}$ for the period 1979–2001. Units: *mm/day*.

Figure 4: Shape parameter estimates $\hat{\nu}$ for October–March wet pentad GPCP precipitation amount from the full model over the period 1979–2001 with the wet pentad threshold set to the 25^{th} percentile.

Figure 5: Standardised SLP parameter estimates for October–March wet pentad GPCP precipitation (a) occurrence $(e^{\hat{\lambda}_1} - 1) \times 100\%$ and (b) amount $(e^{\hat{\kappa}_1} - 1) \times 100\%$ from the full model over the period 1979–2001 with the wet pentad threshold set to the 25^{th} percentile. Units: %. 1-2-1 smoothing applied for lisability. Shading and Solid lines indicate positive contours and dashed lines indicate negative contours. Contour interval is (a) 20 and (b) 10 %.

Figure 6: Saturation specific humidity q_s parameter estimates for October–

March wet pentad GPCP precipitation (a) occurrence $(e^{\hat{\lambda}_2} - 1) \times 100\%$ and (b) amount $(e^{\hat{\kappa}_2} - 1) \times 100\%$ from the full model over the period 1979–2001 with the wet pentad threshold set to the 25^{th} percentile. Units: *% per g/Kg*. 1-2-1 smoothing applied for lisability. Solid lines indicate positive contours with shading and dashed lines indicating negative contours. Contour interval is (a) 20 and (b) 10 *% per g/Kg*.

Figure 7: NAO parameter estimates for October–March wet pentad GPCP precipitation (a) occurrence $(e^{\hat{\lambda}_3} - 1) \times 100\%$ and (b) amount $(e^{\hat{\kappa}_3} - 1) \times 100\%$ from the full model over the period 1979–2001 with the wet pentad threshold set to the 25^{th} percentile. Units: %. 1-2-1 smoothing applied for lisability. Solid lines indicate positive contours starting at 5 % with dashed lines and shading to indicate negative contours starting at -5 %. Contour interval is (a) 10 and (b) 5 % and the zero line has been omitted.

Figure 8: Residual time trend estimates for October–March wet pentad GPCP precipitation (a) occurrence $(e^{\hat{\lambda}_4} - 1) \times 100\%$ and (b) amount $(e^{\hat{\kappa}_4} - 1) \times 100\%$ from the model without SLP, q_s and the NAO with the wet pentad threshold set to $0.1 mm/day$; (c) occurrence and (d) amount from the model without SLP, q_s and the NAO with the wet pentad threshold set to the 25^{th} percentile; (e) occurrence and (f) amount from the full model with the wet pentad threshold set to the 25^{th} percentile. Units: *% per year*. 1-2-1 smoothing applied for lisability. Solid lines indicate positive contours starting at (a, c and e) 1 and (b, d and f) 0.5 *% per year*; dashed lines and shading to indicate negative contours

starting at (a, c and e) -1 and (b, d and f) -0.5 *% per year*; zero line has been omitted and contour interval is (a, c and e) 2 and (b, d and f) 1 *% per year*.

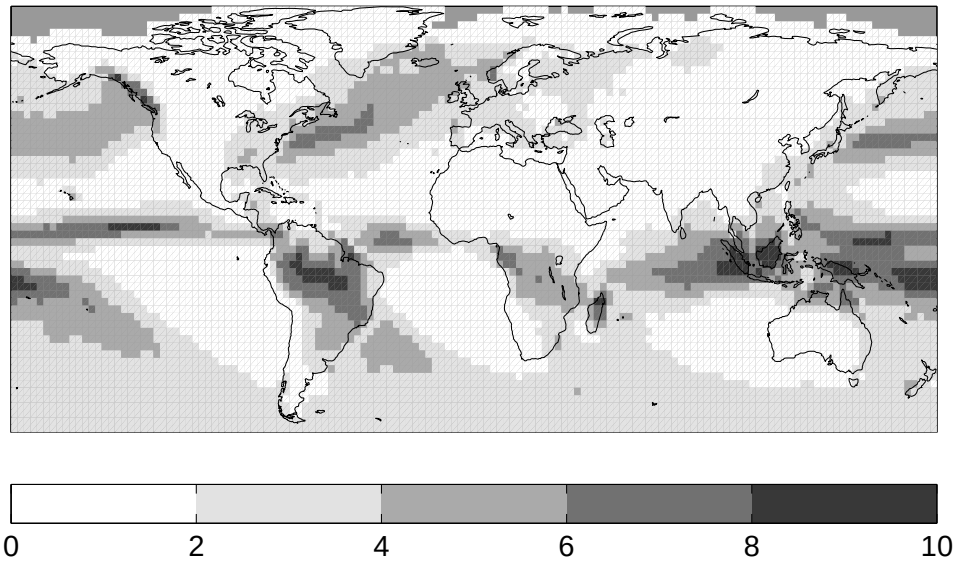

FIG. 1: Long-term mean of October–March winter GPCP pentad precipitation for the period 1979–2001. Units: *mm/day*.

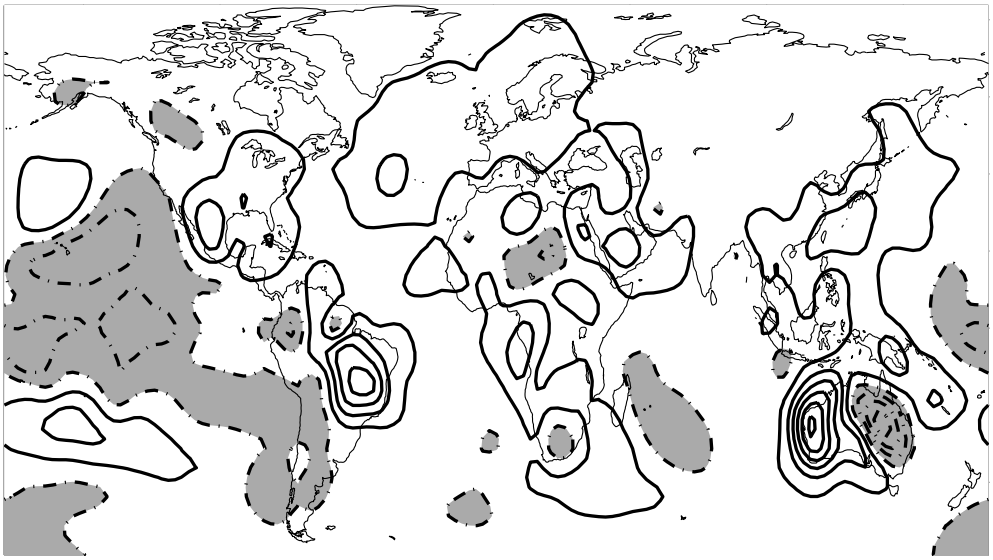

FIG. 2: Long-term linear time trend in October–March saturated specific humidity over the period 1979–2001. Units: *g/kg* per year. 1-2-1 smoothing applied for lisibility. Solid lines indicate positive contours starting at 0.01 *g/kg* with dashed lines and shading to indicate negative contours starting at -0.01 *g/kg*. Contour interval is 0.02 *g/kg* and the zero line has been ommitted.

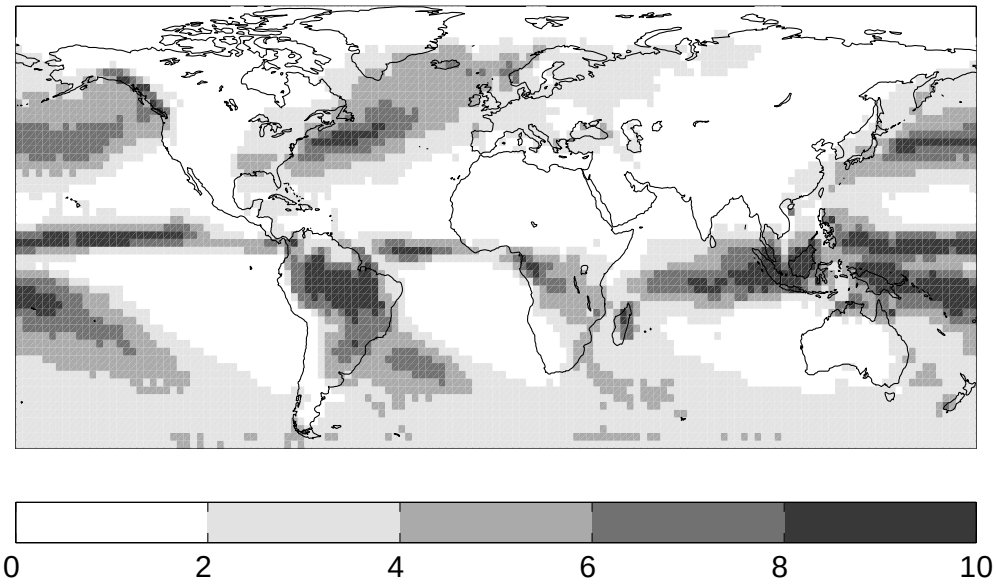

FIG. 3: Long-term mean of October–March winter GPCP wet pentad precipitation amount $e^{\hat{\kappa}_0}$ for the period 1979–2001. Units: *mm/day*.

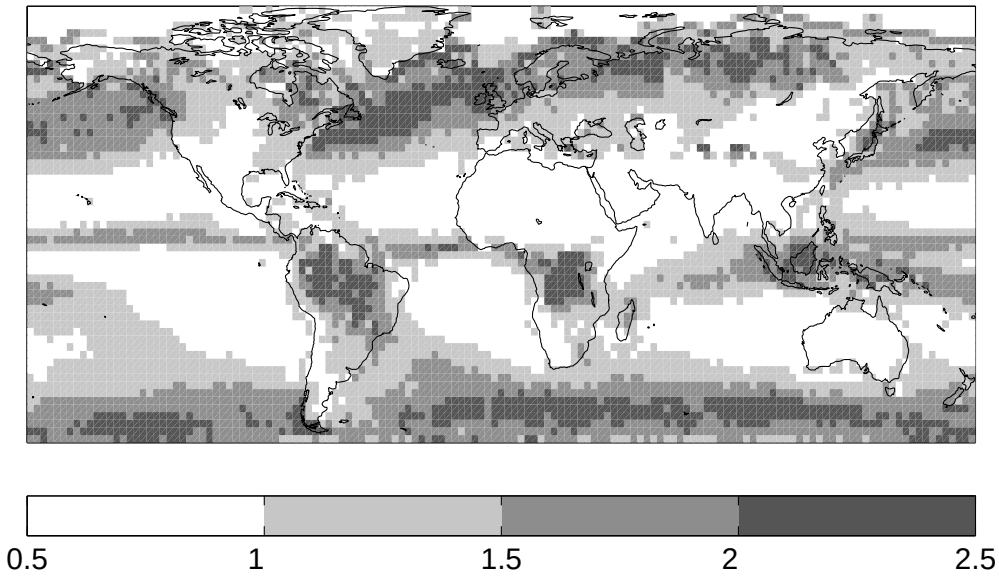

FIG. 4: Shape parameter estimates $\hat{\nu}$ for October–March wet pentad GPCP precipitation amount from the full model over the period 1979–2001 with the wet pentad threshold set to the 25^{th} percentile.

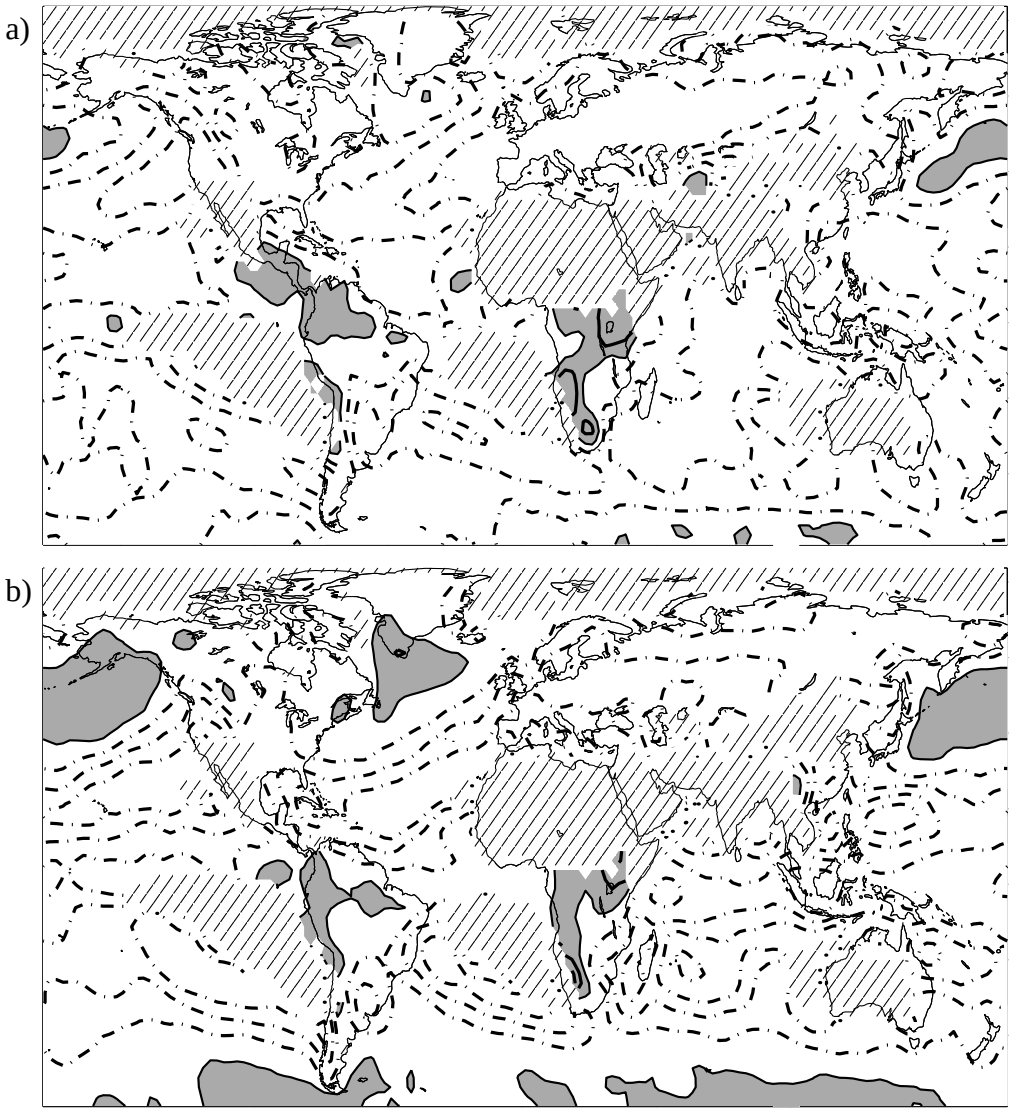

FIG. 5: Standardised SLP parameter estimates for October–March wet pentad GPCP precipitation (a) occurrence $(e^{\hat{\lambda}_1} - 1) \times 100\%$ and (b) amount $(e^{\hat{\kappa}_1} - 1) \times 100\%$ from the full model over the period 1979–2001 with the wet pentad threshold set to the 25^{th} percentile. Units: %. 1-2-1 smoothing applied for lisibility. Shading and Solid lines indicate positive contours and dashed lines indicate negative contours. Contour interval is (a) 20 and (b) 10 %.

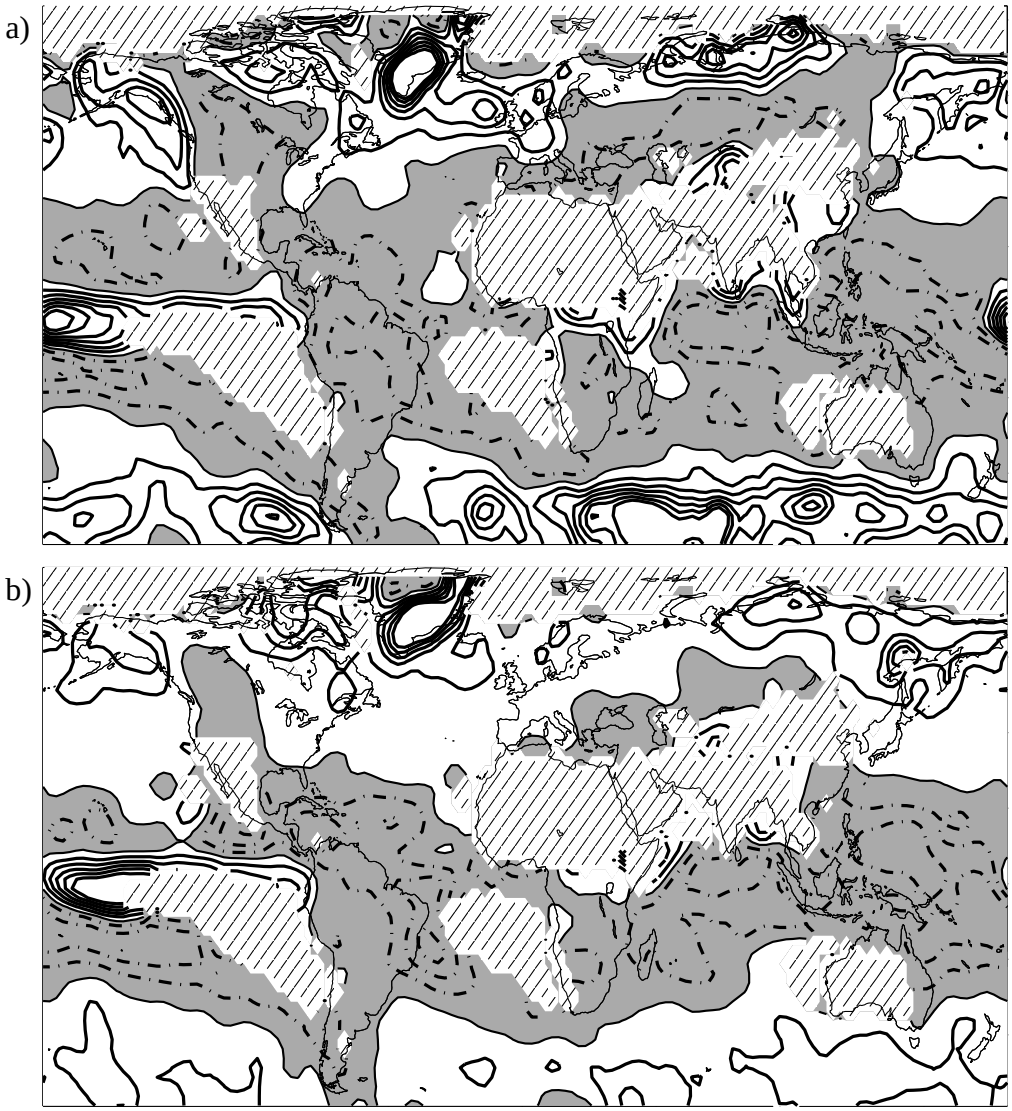

FIG. 6: Saturation specific humidity q_s parameter estimates for October–March wet pentad GPCP precipitation (a) occurrence $(e^{\hat{\lambda}_2} - 1) \times 100\%$ and (b) amount $(e^{\hat{\kappa}_2} - 1) \times 100\%$ from the full model over the period 1979–2001 with the wet pentad threshold set to the 25^{th} percentile. Units: *% per g/Kg*. 1-2-1 smoothing applied for lisibility. Solid lines indicate positive contours with shading and dashed lines indicating negative contours. Contour interval is (a) 20 and (b) 10 *% per g/Kg*.

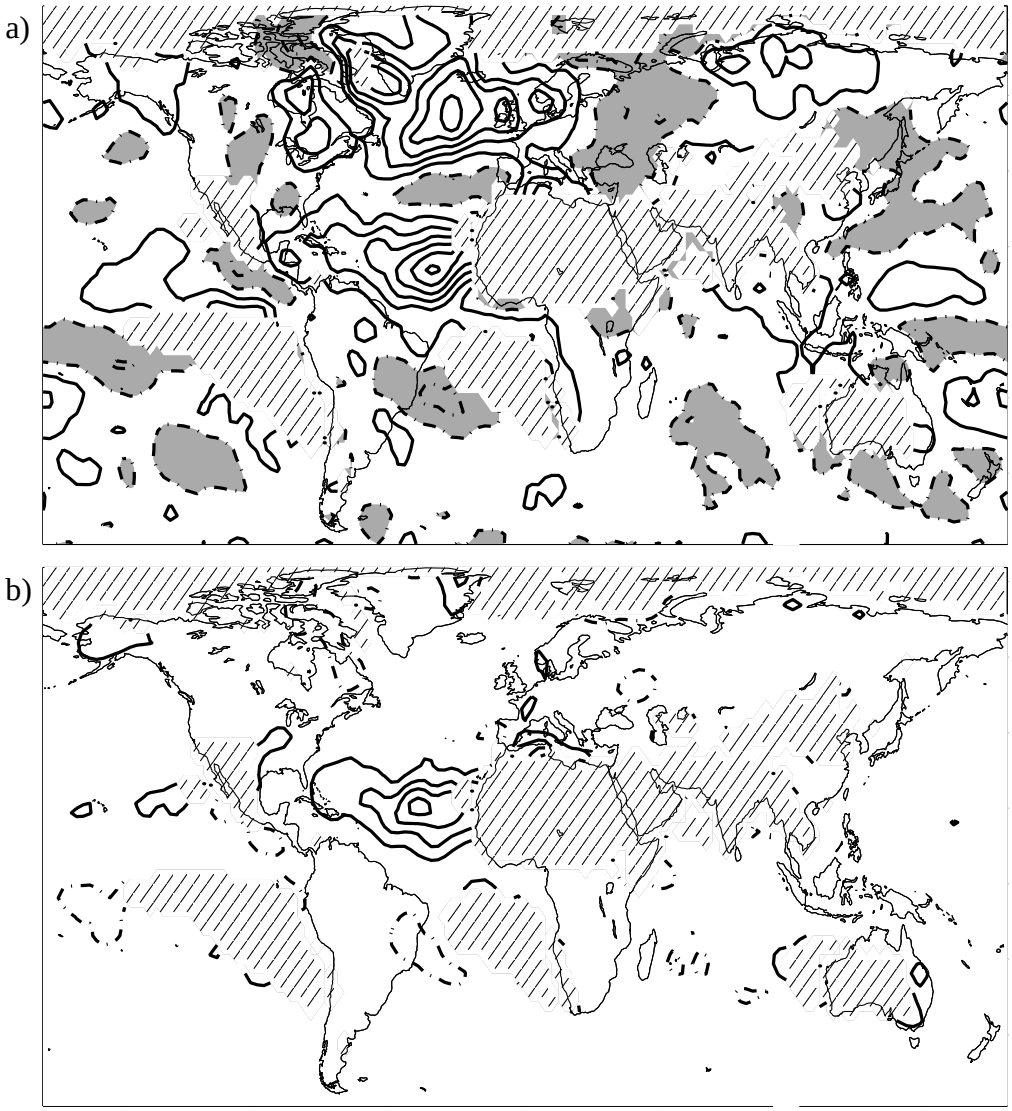

FIG. 7: NAO parameter estimates for October–March wet pentad GPCP precipitation (a) occurrence $(e^{\hat{\lambda}_3} - 1) \times 100\%$ and (b) amount $(e^{\hat{\kappa}_3} - 1) \times 100\%$ from the full model over the period 1979–2001 with the wet pentad threshold set to the 25^{th} percentile. Units: %. 1-2-1 smoothing applied for lisibility. Solid lines indicate positive contours starting at 5 % with dashed lines and shading to indicate negative contours starting at -5 %. Contour interval is (a) 10 and (b) 5 % and the zero line has been ommitted.

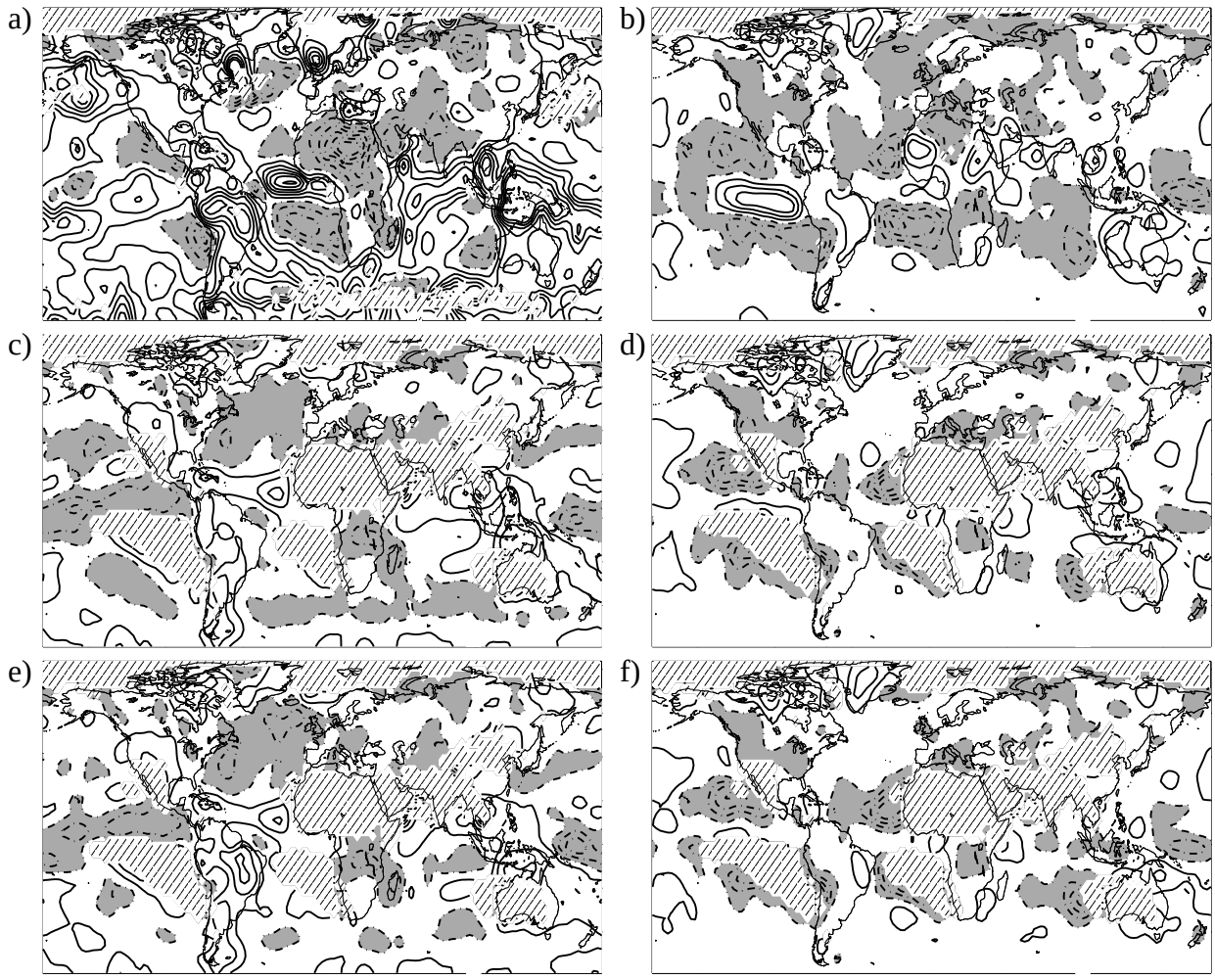

FIG. 8: Residual time trend estimates for October–March wet pentad GPCP precipitation (a) occurrence $(e^{\hat{\lambda}_4} - 1) \times 100\%$ and (b) amount $(e^{\hat{\kappa}_4} - 1) \times 100\%$ from the model without SLP, q_s and the NAO with the wet pentad threshold set to $0.1mm/day$; (c) occurrence and (d) amount from the model without SLP, q_s and the NAO with the wet pentad threshold set to the 25^{th} percentile; (e) occurrence and (f) amount from the full model with the wet pentad threshold set to the 25^{th} percentile. Units: *% per year*. 1-2-1 smoothing applied for lisibility. Solid lines indicate positive contours starting at (a, c and e) 1 and (b, d and f) 0.5 *% per year*; dashed lines and shading to indicate negative contours starting at (a, c and e) -1 and (b, d and f) -0.5 *% per year*; zero line has been ommitted and contour interval is (a, c and e) 2 and (b, d and f) 1 *% per year*.